Semicond. Sci. Technol. **26** (2011) 014031 (8pp) doi:10.1088/0268-1242/26/1/014031

Numerical modeling of intermediate band solar cells

I Tobías, A Luque and A Martí

Instituto de Energía Solar, Universidad Politécnica de Madrid, Ciudad Universitaria, 28040 Madrid, Spain

E-mail: tobias@ies-def.upm.es

Received 31 May 2010, in final form 14 October 2010
Published 9 December 2010
Online at stacks.iop.org/SST/26/014031

Abstract
The performance of intermediate band solar cells under concentrated sunlight is analyzed by means of computer simulation. The continuity equations for electrons and holes and the Poisson equation are numerically solved in one dimension under steady-state conditions. Two situations are considered for a given density of intermediate band centers and optical cross sections. In the first situation, the intermediate band is undoped and a large capture coefficient links conduction and intermediate bands; a large short circuit current enhancement with respect to a conventional cell is obtained, but at the price of strong voltage and efficiency degradation. In the second, the intermediate band is partially filled by doping and there is little thermal contact with the semiconductor bands. The potential of the intermediate band concept is then realized with significant efficiency improvement under highly concentrated illumination. The analysis also reveals that the approximation of flat quasi-Fermi levels is not appropriate.

1. Introduction

The intermediate band (IB) solar cell concept has been proposed [1] as a photovoltaic device capable of very high theoretical efficiency. It is based on the presence of an allowed-energy band within the bandgap of an otherwise conventional semiconductor. This allows transitions between valence and conduction bands to take place via two photons with sub-bandgap energies. To realize a true efficiency enhancement, the current increase must be accompanied by preservation of voltage [2]. The advantages of an IB will be more appreciable under concentrated light.

The IB can be implemented with quantum dots (QDs). This has been the first experimental approach followed [3], and with these prototypes the IB operation principles have been proven [4, 5]. However, these cells featured a low efficiency, mainly because of the low IB absorbance due to the small QD density. Several groups have addressed the technological challenge of increasing the number of QD layers.

The modeling of the IB cell has first been based on detailed balance considerations. Non-idealities were afterwards included to build up an equivalent circuit [3]. To investigate the problem of non-uniform filling of the IB, a flat quasi-Fermi level approximation has been used in which the Poisson equation is solved [6]. The full system of drift-diffusion equations for coupled electrons, holes and IB electrons along with the Poisson equation has also been undertaken [7], with parameters taken from detailed balance principles. Many studies consider the IB as having zero energy-band thickness.

In the QD implementation (and possibly in the bulk material implementation), the charge transport along the IB can be quantitatively unimportant due to the localized nature of the IB centers. If charge transport is ignored and the band is modeled as a discrete level, the equations for the IB cell are the same as for the impurity photovoltaic effect (IPV) [8], which can be modeled with free-distribution software such as SCAPS [9] and AFORS-HET [10].

The objective of this paper is to report on the development of a numerical model for the IB solar cell in one dimension, and to study with it the influence doping the IB layer has on the device performance. At this stage, the IB model is simplified and includes neither transport nor multiple energy levels. After describing the equations and the solution method, a discussion follows on the value of the parameters adopted to describe the simulated structures. Simulations are presented to analyze the different behavior of doped (where the IB is partially filled with electrons in equilibrium) and undoped (where the IB is

initially empty) structures under concentrated light. The paper ends with a summary of conclusions.

2. Numerical model

The system of steady-state differential equations to be solved consists of the carrier continuity equations and the Poisson equation in one dimension:

$$\begin{aligned}\frac{\mathrm{d}J_n}{\mathrm{d}x} &= \frac{\mathrm{d}}{\mathrm{d}x}\left(\mu_n n \frac{\mathrm{d}E_{Fn}}{\mathrm{d}x}\right) = -e\,(G_{\mathrm{BB}} - U_{\mathrm{BB}} + G_{\mathrm{IB}})\\ \frac{\mathrm{d}J_p}{\mathrm{d}x} &= \frac{\mathrm{d}}{\mathrm{d}x}\left(\mu_p p \frac{\mathrm{d}E_{Fp}}{\mathrm{d}x}\right) = e\,(G_{\mathrm{BB}} - U_{\mathrm{BB}} + G_{\mathrm{IB}})\\ \frac{\mathrm{d}^2E_i}{\mathrm{d}x^2} &= \frac{1}{\varepsilon}(n + fN_t - p - N_d).\end{aligned} \tag{1}$$

G_{BB} is the band-to-band (BB) photogeneration rate, U_{BB} is the BB recombination rate including radiative, Read-Hall–Shockley (RHS) and Auger mechanisms, and G_{IB} is the net rate of valence to conduction band transitions through the IB, details of whose calculation are given later.

$N_d(x)$ is the net (shallow) donor concentration, and $N_t(x)$ and $f(x)$ are the concentration of IB centers and their occupancy factor, respectively (as with other magnitudes, the position dependence is not explicitly shown in the formulae). The carrier concentrations are the functions of the quasi-Fermi energies E_{Fn} and E_{Fp} and the intrinsic-level energy E_i:

$$\begin{aligned}n &= n_i \exp\left(\frac{E_{Fn} - E_i}{kT}\right)\\ p &= n_i \exp\left(\frac{E_i - E_{Fp}}{kT}\right).\end{aligned} \tag{2}$$

In the steady state, f must remain constant with time. If no electron transport along the IB takes place, this requires the rate of V→I transitions to be equal at every point to the rate of I→C transitions. This determines the value of f as a function of carrier concentrations and photon-induced transition rates [6]:

$$f = \frac{\sigma_n n + \sigma_p p_t + \gamma_{lp}}{\sigma_n(n + n_t) + \sigma_p(p + p_t) + \gamma_{\mathrm{ln}} + \gamma_{lp}}. \tag{3}$$

From the occupancy factor, an IB quasi-Fermi level is calculated with the Fermi–Dirac distribution function $E_{\mathrm{FIB}} = E_t + kT\ln(f/(1-f))$. The concentrations n_t and p_t are related to the position of the IB level $n_t = n_i^2/p_t = n_i \exp((E_t - E_i)/kT)$. The carrier capture cross sections σ_n and σ_{p} include thermal processes. Formally, they can account for emission and equilibrium light generation, but these are quantitatively unimportant for current devices.

The terms γ_{ln} and γ_{lp} are proportional to the absorption of light by the IB as follows:

$$\begin{aligned}\gamma_{lp} &= \frac{1}{v_{\mathrm{th}}}\int_0^\infty \sigma_{\mathrm{VI}}(E_{\mathrm{ph}})F_{\mathrm{ph}}(E_{\mathrm{ph}})\,\mathrm{d}E_{\mathrm{ph}}\\ \gamma_{ln} &= \frac{1}{v_{\mathrm{th}}}\int_0^\infty \sigma_{\mathrm{IC}}(E_{\mathrm{ph}})F_{\mathrm{ph}}(E_{\mathrm{ph}})\,\mathrm{d}E_{\mathrm{ph}},\end{aligned} \tag{4}$$

where σ_{VI} and σ_{IC} are the optical cross sections of an IB center for the transition indicated by the subindex when the occupation state is favorable, and $F_{\mathrm{ph}}(E_{\mathrm{ph}})$ is the specific photon flux at a given point and photon energy. The position-dependent rate of transitions through IB levels is written as

$$G_{\mathrm{IB}} = N_t \frac{-\sigma_p\sigma_n\left(pn - n_i^2\right) + \sigma_n n_t \gamma_{lp} + \sigma_p p_t \gamma_{ln} + \gamma_{ln}\gamma_{lp}}{\sigma_n(n + n_t) + \sigma_p(p + p_t) + \gamma_{\mathrm{ln}} + \gamma_{lp}}. \tag{5}$$

The photon flux F_{ph} depends on the occupation state of the centers. By neglecting emitted light and confinement effects, this can be calculated as a function of position and energy:

$$\begin{aligned}F_{\mathrm{ph}}(E_{\mathrm{ph}}, x) = F_{\mathrm{ph}}(E_{\mathrm{ph}}, 0)\exp\Bigg(&-\alpha_{\mathrm{BB}}(E_{\mathrm{ph}})x\\ &- \sigma_{VI}(E_{\mathrm{ph}})\int_0^x N_t(x')(1 - f(x'))\,\mathrm{d}x'\\ &- \sigma_{IC}(E_{\mathrm{ph}})\int_0^x N_t(x')f(x')\,\mathrm{d}x'\Bigg).\end{aligned} \tag{6}$$

In order to calculate the photon flux, the occupation of the IB must be known, which in turn depends on the flow of photons through the generation terms. Instead of including this non-local dependence in the semiconductor equations, they are solved separately as explained below.

In this paper we have assumed non-overlapping absorption for the three mechanisms. The band-to-band absorption coefficient is taken from [11], while the optical cross sections σ_{VI} and σ_{IC} of the IB centers are taken as constant over the absorption interval. In our case, with the IB level closer to the conduction than to the valence band, we have

$$\begin{aligned}&\sigma_{\mathrm{IC}} = \sigma_{\mathrm{IC0}} \text{ for } E_C - E_t \leqslant E_{\mathrm{ph}} \leqslant E_t - E_V \text{ and 0 elsewhere.}\\ &\sigma_{\mathrm{VI}} = \sigma_{\mathrm{VI0}} \text{ for } E_t - E_V \leqslant E_{\mathrm{ph}} \leqslant E_G \text{ and 0 elsewhere.}\end{aligned} \tag{7}$$

The flux at the front face follows the AM1.5 Direct 0.1 W cm^{-2} spectral distribution. For IB-mediated transitions, this is integrated over the absorption spectrum since the cross sections are supposed to be constant.

The equations are complemented with Dirichlet boundary conditions for the electrostatic potential and the majority carriers at the contact (imposing equilibrium with electrons in the metal and low injection) and a surface recombination condition for the minority carriers. The p-contact is placed at $x = 0$:

$$\begin{aligned}E_i\,(0) &= E_{FP}(0) + kT\ln\left(\frac{p_{\mathrm{eq}}\,(0)}{n_i}\right)\\ E_{FP}(0) &= 0\\ J_n(0) &= eS_n(n(0) - n_{\mathrm{eq}}(0)).\end{aligned} \tag{8}$$

The second equation sets the potential energy origin at the p-contact metal. For the n-contact at $x = W$, with W the total thickness,

$$\begin{aligned}E_i(W) &= E_{Fn}(W) - kT\ln\left(\frac{n_{\mathrm{eq}}(W)}{n_i}\right)\\ E_{Fn}(W) &= eV\\ J_p(W) &= eS_p(p(W) - p_{\mathrm{eq}}(W)).\end{aligned} \tag{9}$$

Table 1. List of parameters.

Symbol	Case I, undoped IB region, strong CB–IB coupling	Case II, doped IB region, uncoupled CB and IB	Parameter
μ_n	$3000\ \text{cm}^2\ \text{V}^{-1}\ \text{s}^{-1}$		Electron mobility
μ_p	$700\ \text{cm}^2\ \text{V}^{-1}\ \text{s}^{-1}$		Hole mobility
$\tau_p = \tau_n$	10 ns		RHS lifetime
N_D	N_C		n^+ emitter doping
N_A	N_V		p^+ emitter doping
$x_{jn} = x_{jp}$	$0.1\ \mu\text{m}$		n^+ and p^+ emitter thickness
$S_p = S_n$	$10^4\ \text{cm s}^{-1}$		Minority carriers surface recombination velocities
E_C–E_t	0.30 eV		Threshold energy for I→C transitions
E_t–E_V	1.12 eV		*id.* for V→I transitions
E_G	1.42 eV		*id.* for band-to-band transitions
N_t	$10^{18}\ \text{cm}^{-3}$		Density of IB centers
σ_{IC0}	$4.6 \times 10^{-15}\ \text{cm}^2$		Optical cross section I→C transitions
σ_{VI0}	$10^{-14}\ \text{cm}^2$		*id.* for V→I transitions
N_B	$0\ \text{cm}^{-3}$	$5 \times 10^{17}\ \text{cm}^{-3}$	Shallow doping of the IB region
x_{IB}	$0.59\ \mu\text{m}$	$1.18\ \mu\text{m}$	IB region thickness
σ_n	$7.83 \times 10^{-13}\ \text{cm}^2$	$7.83 \times 10^{-18}\ \text{cm}^2$	Cross section for electron capture by IB centers
σ_p	$3 \times 10^{-17}\ \text{cm}^2$	$3 \times 10^{-17}\ \text{cm}^2$	Cross section for hole capture by IB centers

The set of differential equations (1) is discretized and iteratively solved for the quasi-Fermi levels and the intrinsic-level energy. Generation terms are calculated from equation (6) using the previous solution for the energy levels. The scheme described in [11] is followed for the discretization of the continuity equations and the Poisson equation. Newton's method is used to find the new solution using a numerically calculated Jacobian. The matrix is preconditioned by setting diagonal elements equal to 1, and this is found to be important for numerical stability.

After an equilibrium solution is found, for which only the Poisson equation is to be solved, nodes are relocated such that the potential variation between neighboring nodes is at most one-half of the thermal voltage and the distance between them is not greater than a specified value (10 nm near the surfaces). It has been found that further renoding is not necessary. For the structures considered, this leads to 100–150 nodes (and three times as many unknowns).

After each Newton iteration in the solution of the discretized version of system (1), generation terms are updated with equation (6) and new system matrices are calculated for the subsequent step. The convergence test is based on the variation of potential or quasi-Fermi levels between iterations: a variation smaller than 1 nV is generally required; previous checks have shown that this provides enough solution accuracy.

The simple Newton method used here is not able to converge if the trial solution is far from the true one, especially when the equations are strongly coupled by large carrier cross sections and high current levels. Ramping in both light intensity and bias voltage must then be used so that the conditions do not vary very much between successive solutions.

A typical procedure to calculate an *IV* curve would proceed as follows: from the equilibrium state, we start at short circuit at very low illumination levels (10^{-10} suns maybe necessary) that are subsequently raised to the desired concentration by repeated multiplication by ten. More than ten steps can be needed to converge to the new concentration, especially at high current densities for the coupled case. After the short circuit solution is obtained, illumination is held constant while voltage is increased in 10 mV steps, a very conservative value. Four or five iterations are usually enough to find the solution to the next bias point.

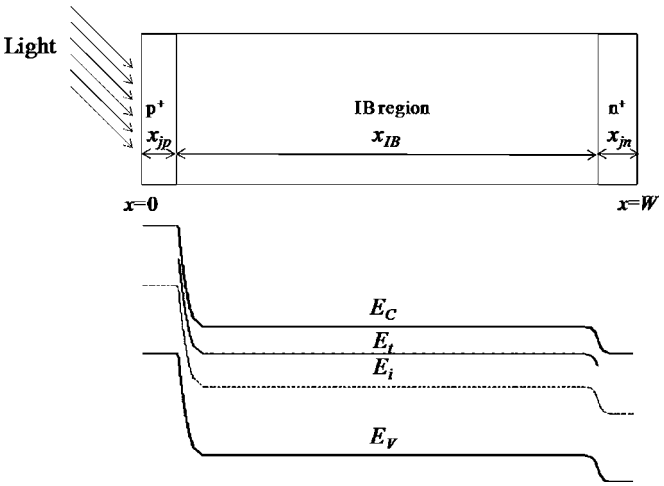

Figure 1. Simulated structure with the schematic band diagram showing the IB level, E_t.

3. Parameters

The simulated structures are GaAs p^+-IB-n^+ diodes with the IB material in the base region, as schematized in figure 1. The transition energies correspond to the InGaAs QDs–GaAs matrix system. GaAs parameters and the standard spectrum are taken from PC-1D [11]. The remaining parameters are set as in table 1, with the two columns corresponding to the two cases discussed in [12]. All parameters and calculations correspond to 25 °C. Regarding the influence of temperature,

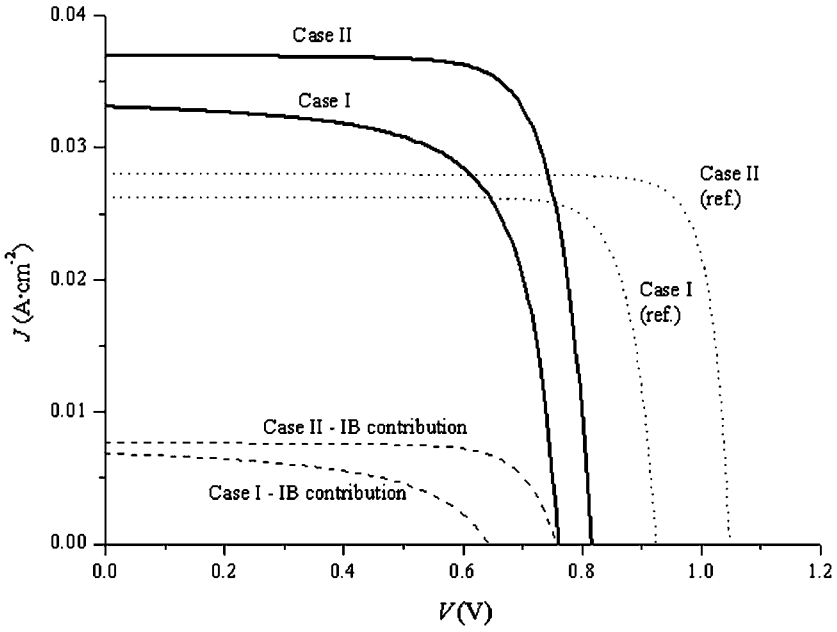

Figure 2. *J–V* curves for case I (undoped) and case II (doped) in table 1 at 1 sun (solid lines). The long-dashed lines give the IB contribution when it is positive (i.e. net photogeneration). The short-dashed lines correspond to reference devices that have no IB centers but otherwise are identical to cases I and II, respectively.

the difference with conventional cells would lie on the behavior of thermal and optical capture cross sections by IB centers, which is not well known. The former are likely increasing with temperature as for other impurities or recombination centers, while the latter are less dependent on it, and one would expect a similar behavior to conventional cells at operation temperatures.

The first case corresponds to a structure without base doping and with strong coupling between conduction and intermediate bands via a large thermal capture cross section. This large capture coefficient may be related to the existence of localized states with higher energies.

In the second case considered, the IB region is doped to half-fill the centers and the thermal coupling with semiconductor bands is very weak. The thickness of this structure has been tailored so that generation through the IB is more or less the same for both cases.

The values of γ_{ln} and γ_{lp} were obtained in [6] from the fit of quantum efficiency and electroluminescence in prototype solar cells with a very thin IB region. They are converted here to cross section values using (4) and the number of photons in the considered wavelength range of the solar spectrum.

Reference structures are also considered that are identical to those in table 1, except that they have no IB centers in the base region.

4. Simulation results

Figure 2 shows the *J–V* curves at 1 sun concentration for the two cases in table 1 along with the reference cells. Note that the doped (case II) cell has a larger BB generation due to the increased thickness, as is also apparent by comparing the reference devices. BB photogeneration current densities are 26.3 (case I) and 29.5 mA cm^{-2} (case II). IB photogeneration contributes 6.9 and 7.7 mA cm^{-2}, respectively, at short circuit. The voltage of the doped cell is much lower than that of the reference because of recombination via IB centers. Low fill factors affect all devices, including the references, because RHS recombination in the space charge region is dominant among recombination losses not related to the IB. The current generation via the IB is high for the undoped cell too, giving an improved short circuit current with respect to BB photogeneration. However, the open circuit voltage is very much degraded due to the large IB capture cross section for electrons. Efficiency values for these structures are given in table 2. It can be seen that no improvement is derived from the IB at 1 sun because the short circuit current improvement does not compensate for the voltage degradation.

Table 2. Simulated efficiencies (%) of different IB devices (0.1 W cm^{-2} AM 1.5D, 25 °C).

Concentration factor	Case I	Case I (ref.)	Case II	Case II (ref.)
1×	17.13	19.88	23.30	25.12
1000×	3.25	27.06	34.47	30.92

The way the IB current increment is obtained is different in both cases: in the undoped case, the centers are empty, so that the V→I transition is favored. The second transition is produced thermally due to the strong coupling with the conduction band via σ_n, thus completing the generation of free carriers. In the doped case, the IB is half-filled and both optical transitions proceed more or less at the same rate.

This can be seen in figure 3, where energy band diagrams at short circuit, the rates of different transitions to and from

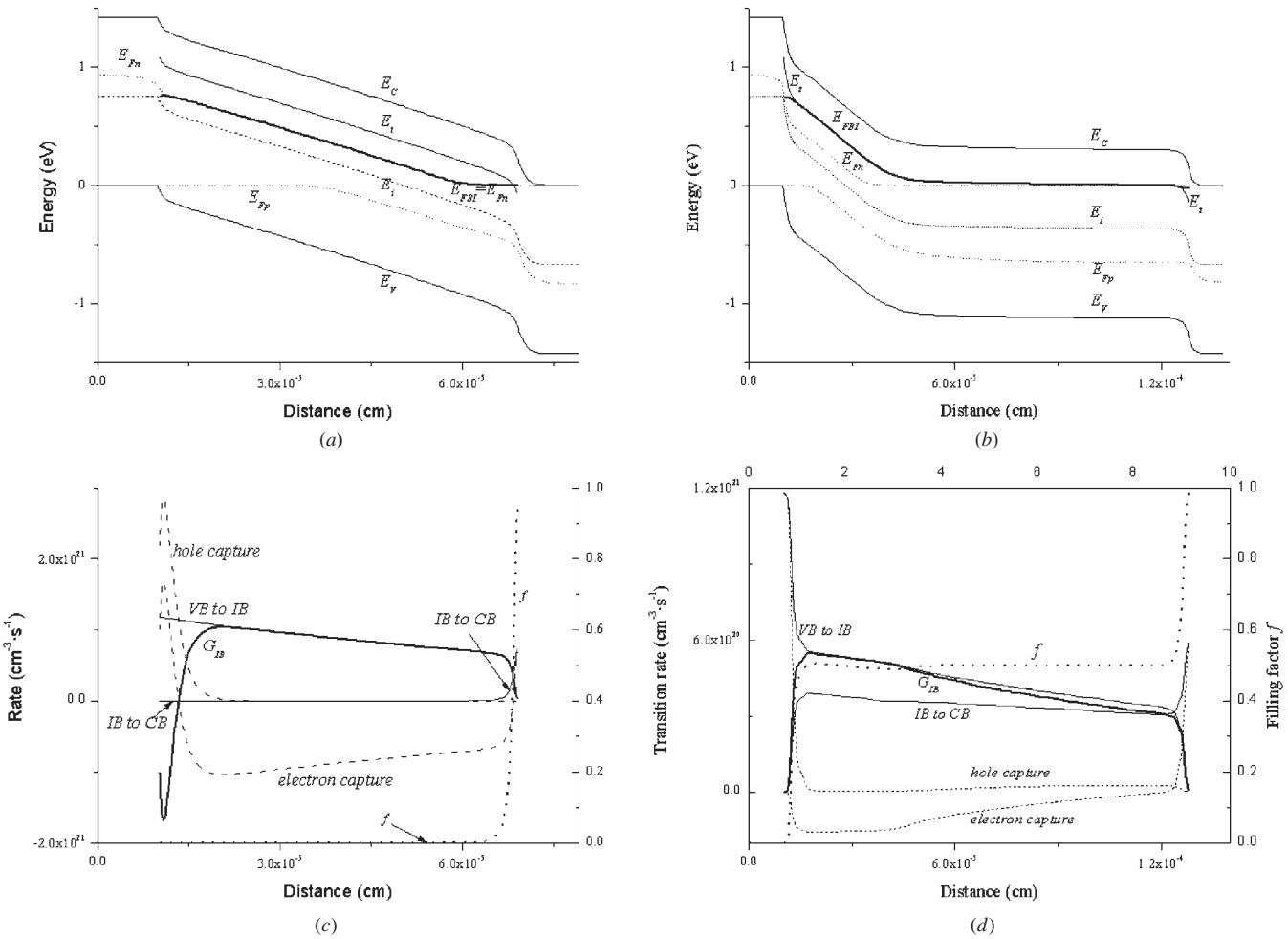

Figure 3. Energy band diagrams ((*a*) and (*b*)) and transition rates plus IB occupancy factor ((*c*) and (*d*)) for the simulated structures at 1 sun. (*a*) and (*c*) Undoped, coupled (case I). (*b*) and (*d*) Doped, uncoupled (case II).

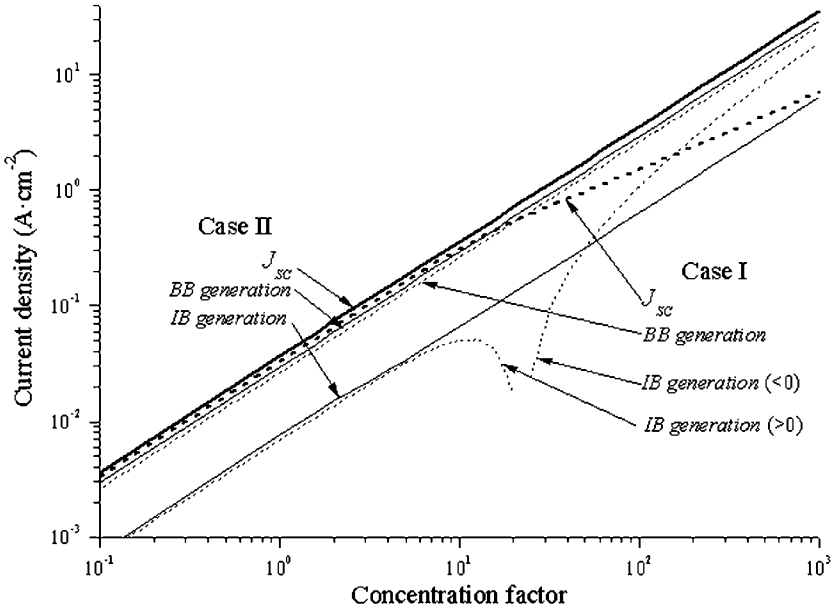

Figure 4. External cell current and generation currents at short circuit as a function of the concentration factor. The dotted lines: case I in table 1. The solid lines: case II. The thick lines represent the external current; the thinner lines stand for the band-to-band (BB) photogeneration and for the generation via the IB, in absolute values. For case I, the IB contribution becomes zero at around 20× and is then negative, i.e. recombination via the IB is larger than the corresponding generation.

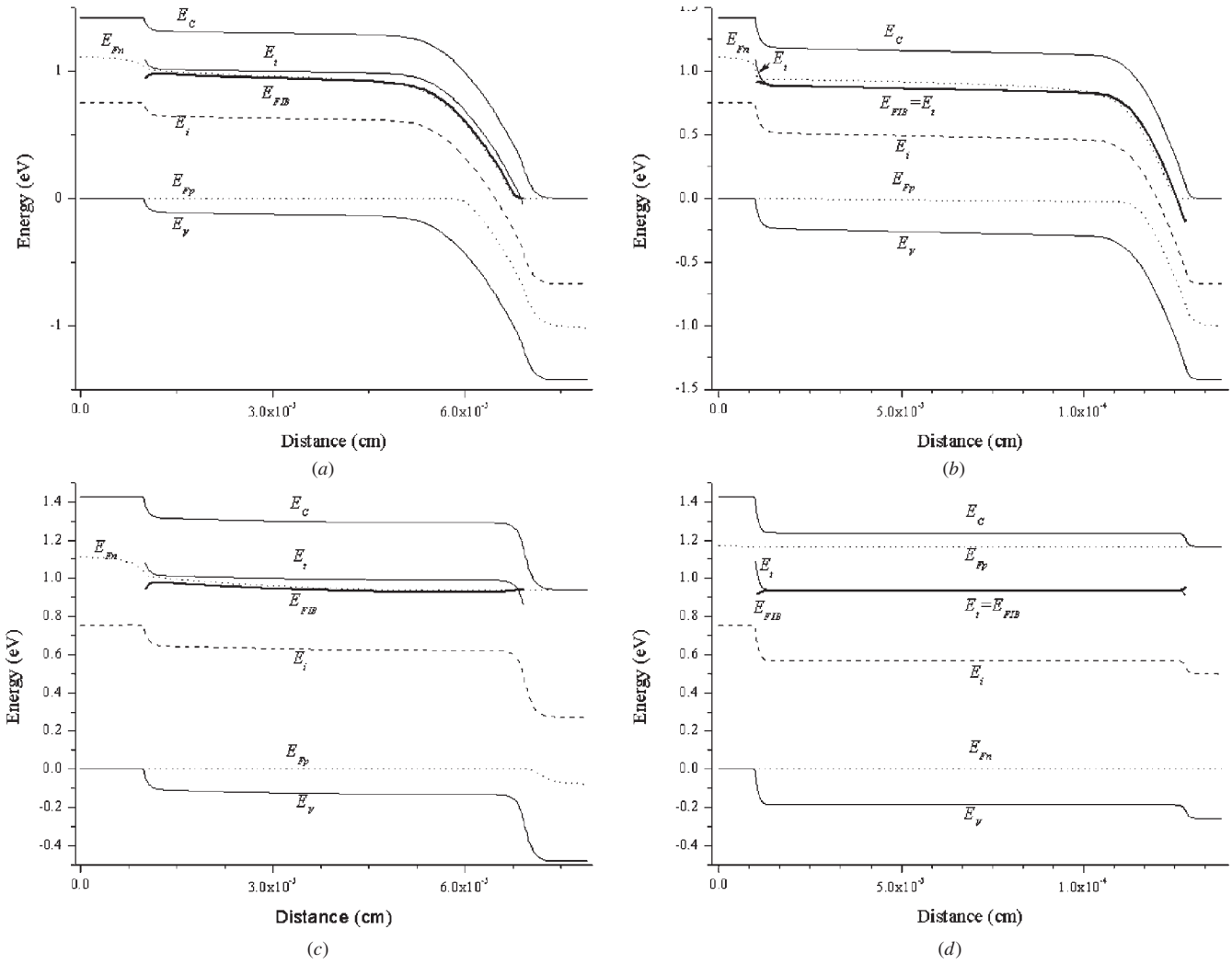

Figure 5. Energy band diagram at 1000 suns concentration. Short circuit: (*a*) and (*b*); open circuit: (*c*) and (*d*). Case I: (*a*) and (*c*); case II: (*b*) and (*d*). The solid thin lines represent semiconductor band edges and the IB level. The dashed line represents the intrinsic level. The dotted lines stand for the CB and VB quasi-Fermi levels, while the thick line is for the IB Fermi level.

the IB and the occupancy factor of the centers are presented. In the undoped case (I), the IB is empty and within the cell space charge region. Photogeneration from valence to IB is strong, while the complementary transition is suppressed. It is also apparent that the IB centers are emptied by thermal emission (a negative electron capture rate appears in the graph) to the conduction band: note that the quasi-Fermi levels for electrons in the conduction and intermediate bands coincide except near the emitters. For case II, the half-filled IB is largely inside a neutral zone and the quasi-Fermi level lies at the energy level of the band center. Both photogenerated transitions are important. Doubling the base thickness has the purpose of compensating for the fact that the concentration of empty centers is now half the total concentration. In this way the same current increase is roughly obtained.

Figure 4 shows the short circuit current density–concentration plot for both structures. The band-to-band and IB-mediated generation currents are also shown. It can be seen that the IB provides substantial current increase at low concentrations, as previously commented. In the flat quasi-Fermi level approximation, all current contributions would be linear with concentration because without Fermi level separation no recombination takes place. When carrier transport equations are included, the situation is very different: recombination becomes very intense for the coupled case at moderate concentrations, causing the IB generation to become negative and producing a strong sublinear behavior of the short circuit current.

Figure 5 shows the short circuit band diagram at 1000 suns concentration. The large quasi-Fermi level split affects the ionization of the IB for the undoped case, as can be seen since E_{FIB} follows the electron level. Contrarily, for the doped case, the occupancy of the IB is still close to 1/2 in most of the region. Note that in both cases most of the potential barrier develops at the n^+ emitter space charge region, i.e. the IB region becomes p type.

The approximation of flat quasi-Fermi levels is more accurate under open circuit conditions, but for case I structures, the differences can be important. This can be appreciated in figures 5(*c*) and (*d*). Band diagrams at open circuit for both

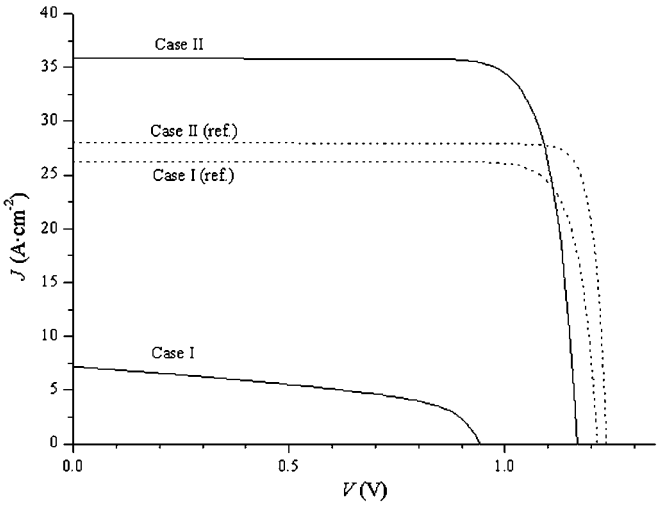

Figure 6. *J–V* curves for case I (undoped) and case II (doped) in table 1 at 1000 suns (solid lines). The dashed lines correspond to reference devices that have no IB centers but otherwise are identical to cases I and II, respectively.

cases and 1000× concentration are presented. While for case II the conduction and valence band Fermi energies do not vary across the base, for case I there is still a significant curvature which is a consequence of the strong link between the charge state of the centers and the electron concentration.

At 1000 suns, as can be seen in figure 6, the doped, uncoupled cell performs very well, exhibiting substantial current increase without much voltage degradation as compared to the reference device. As given in table 2, a significant efficiency increase is achieved in accordance with the IB solar cell principles. The undoped, coupled structure, on the other hand, shows a deeply degraded performance both in voltage and current.

5. Conclusions

A computer code for simulating IB solar cells in one dimension has been developed. It is based on the numerical solution of the electron and hole continuity equations and the Poisson equation. The IB is modeled as a gap energy level that exchanges electrons with the semiconductor bands. No electron transport along the IB is considered.

Two solar cell structures have been simulated. Both feature a similar short circuit current increment at low concentration due to the IB; however, the open-circuit voltage and behavior under concentration are very different. In the first structure, the sub-bandgap current is large with an empty IB because the generation is completed via a strong thermal coupling of the intermediate and conduction bands; however, this implies large recombination under forward bias. Consequently the voltage is low and the current responsivity decreases steeply with concentration. In the second structure both sub-bandgap transitions are light-induced. This leads to much better performance, although the IB must be thicker to achieve the same current as in the previous case.

While the ideal, detailed balance efficiency limit of IB solar cells is 63.2%, it is lower (30.2 and 51.6% at 1 and 1000×, respectively) [13] for the transition energies for the InAs/GaAs system considered here. The values obtained in this study (25.1 and 30.9% for case II) include the effect of non-radiative recombination, limited mobility and incomplete absorption, but not band non-idealities or photon recycling. They could approach what could be achieved without light management techniques if the thermal capture coefficients between the IB and the host bands were minimized.

This work is intended as an indication to technologists that the short circuit current cannot be the only figure of merit in the development of a high-efficiency IB solar cell, and that pre-filling the band by doping is necessary for current collection in good devices.

Acknowledgments

This work is supported by the European Commission within the project IBPOWER (Contract 211640), the project NUMANCIA (S2009/ENE/1477) funded by the Comunidad de Madrid and the project GENESIS-FV (CSD2006-00004) funded by the Spanish National Program.

References

[1] Luque A and Martí A 1997 Increasing the efficiency of ideal solar cells by photon induced transitions at intermediate levels *Phys. Rev. Lett.* **78** 5014–7
[2] Luque A and Martí A 2001 A metallic intermediate band high efficiency solar cell *Prog. Photovolt.* **9** 73–86
[3] Luque A, Martí A, Stanley C, López N, Cuadra L, Zhou D and Mc-Kee A 2004 General equivalent circuit for intermediate band devices: potentials, currents and electroluminescence *J. Appl. Phys.* **96** 903–9
[4] Martí A, Antolín E, Stanley C, Farmer C, López N, Díaz P, Cánovas E, Linares P G and Luque A 2006 Production of photocurrent due to intermediate-to-conduction-band transitions: a demonstration of a key operating principle of the intermediate-band solar cell *Phys. Rev. Lett.* **97** 247701–4
[5] Luque A, Martí A, López Antolín E, Cánovas E, Stanley C, Farmer C, Caballero L J, Cuadra L and Balenzategui J L 2005 Experimental analysis of the quasi-Fermi level split in quantum dot intermediate-band solar cells *Appl. Phys. Lett.* **87** 083505
[6] Luque A, Martí A, López N, Antolín E, Cánovas E, Stanley C, Farmer C and Díaz P 2006 Operation of the intermediate band solar cell under nonideal space charge region conditions and half filling of the intermediate band *J. Appl. Phys.* **99** 094503
[7] Lin A S, Wang W and Phillips J D 2009 Model for intermediate band solar cells incorporating carrier transport and recombination *J. Appl. Phys.* **105** 064512
[8] Keevers M J and Green M A 1994 Efficiency improvements of silicon solar cells by the impurity photovoltaic effect *J. Appl. Phys.* **75** 4022–31
[9] Khelifia S, Verschraegen J, Burgelman M and Belghachia A 2008 Numerical simulation of the impurity photovoltaic effect in silicon solar cells *Renew. Energy* **33** 293–8
[10] Stangl R, Kriegel M and Schmidt M 2006 AFORS-HET, Version 2.2, a numerical computer program for

simulation of heterojunction solar cells and measurements *Proc. 4th World Conf. on Photovoltaic Energy Conversion* pp 1350–3

[11] Clugston D A and Basore P A 1997 PC-1D version 5: 32-bit solar cell modeling on personal computers *Proc. 26th Photovoltaic Specialists Conf.* pp 207–10 Available at http://www.pv.unsw.edu.au/links/products/pc1d.asp

[12] Luque A and Martí A 2010 On the partial filling of the intermediate band (IB) in IB solar cells *IEEE Trans. Electron Devices* **57** 1201–7

[13] Martí A, Antolín E, Cánovas E, López N, Linares P G, Luque A, Stanley C R and Farmer C D 2008 Elements of the design and analysis of quantum-dot intermediate band solar cells *Thin Solid Films* **516** 6716–22